ANL-HEP-TR-93-89
December 1993

$W^{\pm}$ and Z^0 Event Rates and Background Estimates for the STAR Detector at RHIC in pp Collisions

V. L. Rykov[1] and K. E. Shestermanov[2]
Visitors to BNL from IHEP
Protvino, Russia

Abstract

The estimates for $W^{\pm}$ and Z^0 production rates and various background contributions in the **STAR** detector with the barrel electromagnetic calorimeter are presented. These results were obtained by Monte-Carlo simulations with the *PYTHIA V5.6/JETSET V7.3* of the *LUND* set of routines and *GEANT V3.15*.

[1]This research was supported in part by the U.S. Department of Energy, Division of Basic Energy Sciences under contract no. DE-AC02-76CH00016.
[2]Work supported in part by the U.S. Department of Energy, Division of High Energy Physics, Contract W-31-109-ENG-38.

1 Introduction

In this paper, we continue to study the feasibility of detecting $W^{\pm}$ and Z^0 with the **STAR** detector [1, 2] at RHIC. Estimates for the event rates [3, 4] had shown that, in pp collisions at $\sqrt{s} = 500\, GeV$ for the integrated luminosity $800 pb^{-1}$, the **STAR** detector with the electromagnetic calorimeter (*EMC*) [1, 2] is able to collect about 10^5 $W^{\pm} \rightarrow e^{\pm}\nu$ events and several thousands of $Z^0 \rightarrow e^+e^-$ decays. Here we present estimates for various background sources to the process $pp \rightarrow W^{\pm} + X \rightarrow e^{\pm}\nu + X$. The results were obtained by Monte-Carlo simulations with the *PYTHIA V5.6/JETSET V7.3 LUND* programs [5] and *GEANT V3.15* [6]. The *EHLQ1* [7] set of proton structure functions has been used. As in [4], all parameters in *PYTHIA* were set to their default values except for two. The choices for the $MSTP(2)$ and $MSTP(33)$ were as following:

$MSTP(2) \;\; = 2$ Second order running α_s;

$MSTP(33) = 2$ Separate K factors are used for ordinary ($PARP(31) = 1.5$) and color annihilation graphs ($PARP(32) = 2.0$).

Inclusive $W^{\pm}$ and Z^0 production cross sections values derived here from *PYTHIA V5.6* are essentially the same as in [4], while detecting efficiencies and event rates are slightly different. The reason is that the old *PYTHIA V5.3* version [8] used earlier [4] did not provide a correct description of the $W^{\pm}$ and Z^0 polarization states and consequently the correct kinematics for the leptons produced from their decays.

2 STAR Detector

The **STAR** detector (Fig. 1) at RHIC had been described elsewhere [1, 2]. With a barrel electromagnetic calorimeters *(EMC)* **STAR** is especially suitable for detecting W and Z bosons [4, 9] due to its large acceptance in the central rapidity region for the electrons produced by high-mass particles decays.

The proposed barrel EMC [2] is a lead-scintillator sampling calorimeter. It is located inside the aluminium coil of the **STAR** solenoid magnet and covers $|\, \eta \,| \leq 1.05$ and 2π in azimuth, thus matching the acceptance for full Time Projection Chamber (*TPC*) tracking. The inner radius is 2.20 meters and the overall length is 6.20 meters. It consists of 120 modules with 21 layers of 4-mm thick plastic scintillator and 20 layers of 5-mm thick lead plates. This corresponds to a total of approximately 20 radiation lengths (X_0), including a 20-mm thick aluminium front plate. The *EMC* segmentation will be $\Delta\varphi = 0.1$ and $\Delta\eta = 0.1 - 0.2$. At $\eta \sim 0$, the total amount of material in front of the *EMC* is $\sim 0.5 \cdot X_0$.

A Shower Maximum Detector *(SMD)* with a fine spatial resolution will be placed at a depth of approximately $5 \cdot X_0$. A number of versions for the *SMD* design are currently under investigation at IHEP, Protvino [10]. Here it has been assumed the *SMD* consists of 24-cm long scintillator rods with the transverse size of 1x1 cm^2. The radial space allotted is 25 mm.

The *EMC* energy resolution for $e^{\pm}$ obtained by Monte Carlo calculations is approximately equal to

$$\sigma_E/E = 20\%/\sqrt{E}, \tag{1}$$

where E is in GeV. The momentum resolution of the **STAR** tracking system (*TPC* only) is expected to be [1]:

$$\sigma_P/P = 1.0\% \cdot P, \tag{2}$$

where P is in GeV/c.

3 Production Cross Sections and Event Rates

PYTHIA V5.6 program provides the following estimates for W and Z production cross sections in pp interactions at $\sqrt{s} = 500\,GeV$:

$$\sigma \cdot B(pp \to W^+ + X \to e^+\nu_e + X) = \mathbf{120}\,pb,$$
$$\sigma \cdot B(pp \to W^- + X \to e^-\overline{\nu}_e + X) = \mathbf{43}\,pb,$$
$$\sigma \cdot B(pp \to Z^0 + X \to e^+e^- + X) = \mathbf{10}\,pb.$$

The pseudorapidity distributions for electrons and positrons from $W^{\pm}$ decays are shown in Fig. 2. Positrons from W^+ are more concentrated in the central rapidity region, while electrons from W^- are more spread out in η due to the polarization properties of the gauge bosons generated in pp collisions, which then decay due to the parity violating weak interaction. So, one should expect the detecting efficiency for W^+ to be higher than for W^-. The P_T^e spectra for decay electrons and positrons from $W^{\pm}$ are shown in Fig. 3, and for the highest P_T electron from Z^0 decays shown in Fig. 4.

Expected event rates in **STAR** for an integrated luminosity of $\int L\,dt = 8 \cdot 10^{38}\,cm^{-2} = 800\,pb^{-1}$ ($L = 2 \cdot 10^{32}\,cm^{-2} \cdot sec^{-1}$ times $4 \cdot 10^6\,sec$ which correspond to 100 days with the 50% efficiency) are presented in Table 1 for several values of triggering cuts applied to the $e^{\pm}$ transverse momentum P_T^e. An event is considered a candidate for the W decay if $P_T^e > P_T^e\_cut$. For Z^0 events the same requirement has been applied for at least one of two decay electrons.

It has also been taken in account that the fiducial *EMC* acceptance is usually smaller than the one defined by the design geometry, due to excluding events with $e^{\pm}$ hits in some area close to *EMC* edges. This is reflected in Table 1b, where the numbers correspond to the reduced acceptance of $|\eta| \leq 0.95$.

Table 1. Event rates for $pp \to W^{\pm} + X \to e^{\pm}\nu_e + X$ and $pp \to Z^0 + X \to e^+e^- + X$ at $\sqrt{s} = 500\,GeV$ for $\int L\,dt = 8 \cdot 10^{38}\,cm^{-2} = 800\,pb^{-1}$

a) $|\eta| \leq 1.05$ acceptance

$P_T^e\_cut$, GeV/c	10	15	20	25	30	35	40	45	50
W^+	74,080	72,340	67,900	60,250	48,600	32,670	9,190	1,160	250
W^-	16,930	16,890	16,620	15,910	14,280	10,780	3,050	380	90
Z^0	3,140	3,140	3,140	3,140	3,135	3,085	2,575	1,460	200

b) $|\eta| \leq 0.95$ acceptance

$P_T^e\_cut$, GeV/c	10	15	20	25	30	35	40	45	50
W^+	69,850	68,500	64,600	57,560	46,560	31,130	8,700	1,090	240
W^-	15,200	15,170	15,000	14,470	13,120	9,900	2,890	360	80
Z^0	2,660	2,660	2,660	2,660	2,660	2,610	2,295	1,330	190

The geometrical acceptance for the $|\eta| \leq 0.95$ is 72% for W^+, 44% for W^- and 33% for Z^0.

4 Background to $W^{\pm}$

Any event with a high, local energy deposition in the *EMC/SMD*, matching a high-P_T charged particle, and observed in the tracking system, may be considered a potential candidate for a $W^{\pm}$ decay. Other sources can also provide such a signature.

In this section we provide estimates for the background to $W^{\pm}$ in **STAR** originating from the following sources:

– Z^0 events with one missing electron;
– electrons from π^0 Dalitz decays;
– misidentified high-P_T charged hadrons as electrons;
– overlapping in the *EMC/SMD* γ-quanta from π^0 decays with charged high P_T hadrons.

4.1 Z^0 with one missing electron

A background from $Z^0 \rightarrow e^+e^-$ with one electron missing cannot be rejected, in principle. For an integrated luminosity of $800\,pb^{-1}$, the expected number of events with a missing e^-, but detected e^+ in the fiducial acceptance is about 1700, and the same number of events with a missing e^+, but detected e^-. Thus, a background from Z^0 decays to W^+ will be ~2.5%, and for W^- – about 11%. The $P_T^{e\pm}$ spectrum for this background is shown in Fig. 5 along with the $e^{\pm}$ spectra from $W^{\pm}$ decays.

4.2 Dalitz pairs

The upper limits for the background from π^0 Dalitz decays to $W^{\pm}$ at various $P_T^e\_cut$ values are presented in Table 2. We assume that an event with one or more Dalitz pair from $\pi^0 \rightarrow \gamma e^+e^-$ contributes to the background of either W^+ or W^- if at least one decay electron or positron with $P_T^e > P_T^e\_cut$ hits the *EMC* within its fiducial acceptance. No other cuts were applied. All event rates in Table 2 are normalized to the W^+ event rate with the $P_T^e\_cut = 10\,GeV/c$ for the *EMC* acceptance $|\eta| \leq 0.95$.

Table 2. Upper limits for the background from π^0 Dalitz decay.

P_T^e_cut, GeV/c	W^+	W^-	Background to W^+ (or W^-) from Dalitz decays
10	1.00	0.22	0.59
15	0.98	0.22	0.11
20	0.93	0.21	0.02
25	0.82	0.21	0.005

We observe that even with the only requirement being $P_T^e > 20 - 25\, GeV/c$, the background from Dalitz pairs is at the same level or even lower than from Z^0 decays, while the detecting efficiencies for $W^{\pm}$ drop only by 7-18%. Taking into account that applying such criteria to the W selection as an isolation cut, rejecting pairs of close proximity $e^{\pm}$, distinguishable in the tracking system and with *SMD*, a background from π^0 Dalitz decays may be considered negligible.

4.3 Misidentified high-P_T charged hadrons

The contamination of the $W^{\pm}$ event sample by high-P_T charged hadrons misidentified as electrons is expected to be the most serious source of background. One can see from Table 3 (see also Figs. 8–10) that the number of events with a high-P_T π^+ or proton is well above the number of $W^{\pm}$ events [3]. So, an ability to extract $W^{\pm}$ signals depends on the detector capability to distinguish a charged hadron from an electron.

Table 3. Relative number of generated events with high P_T positive hadrons normalized to the W^+ event rate with P_T^e_$cut = 10\, GeV/c$.

P_T_cut, GeV/c	No Cuts		
	W^+	W^-	Positive hadrons
10	1.00	0.22	3,600
15	0.98	0.22	500
20	0.93	0.21	75
25	0.82	0.21	20
30	0.66	0.19	6
35	0.45	0.14	2.2

A number of the **STAR** detector features can be used to separate charged hadrons from electrons. Most of the selection criteria, discussed below, have been used before in other collider experiments.

At the lowest trigger level a threshold of about 20-25 GeV/c should be applied to the $P_T^{e\pm}$, measured as a weighted sum of signals in the adjacent *EMC* towers. Since hadrons

[3]In this paper we did not study specially the background from negative hadrons, but assumed, that it is at the same level or even lower, than the positive one. So, the background curves at Figs. 8-10 and numbers in Tables 3, 4 in respect to W^- should be considered rather as the upper limits.

mostly deposit only a fraction of their energy in the *EM* calorimeter, a single hadron will effectively be "seen" in the *EMC* as a particle with a lower P_T than it actually is. Thus, due to the rapid drop of the hadron P_T spectrum when P_T increases, it effectively provides a hadron P_T spectrum, measured in the *EMC*, lying well below the actual one. In Fig. 6 one can see how it works. The effective hadron suppression power of this mechanism varies from about 50 to 150 in the P_T region of 10 – 50 GeV/c.

However, high-P_T hadrons usually originate from jets. And, since the proposed *EMC* for **STAR** is not fine-grained, particles surrounding a high-P_T charged hadron can significantly increase an effective *EMC* response in adjacent towers. So, at further analysis stages the information from the tracking system and a fine-grained *SMD* should be used for the jets recognition.

In this first pass for the background study the following criteria for high-P_T $e^{\pm}$ selection have been applied:

Energy-Momentum matching. A charged particle was considered a hadron and thus rejected, if its momentum, measured in the tracking system, did not match its energy, as measured in the *EMC*, within $2 \cdot \sqrt{\sigma_E^2 + \sigma_P^2}$, where σ_E and σ_P are from eq. (1) and (2). Actually, if the tracking system consists only of the *TPC* with σ_P from eq. (2), this criterion has a rejection power ~ 5 at P_T just above 10 GeV/c, which then goes down rapidly due to the momentum resolution deterioration at higher P_T (see Fig. 7).

Isolation cut. An electron candidate was considered as originating from a $W^{\pm}$ decay, if the sum $E_{EMC} + E_{charged}$, detected in the cone $\Delta R = \sqrt{(\Delta\eta)^2 + (\Delta\varphi)^2} = 0.7$ and centered around an $e^{\pm}$ candidate, was less than $0.1 \cdot E_e$. Here E_{EMC} is the energy deposited in the *EMC* by all particles except a high P_T electron; $E_{charged}$ is a sum of all charged-particle energies (excluding an $e^{\pm}$ candidate), measured in the tracking system; E_e is the energy of the $e^{\pm}$ candidate.

Shower width. With the *SMD* it is possible to measure a transverse width of showers and reject those of them, which are spread more than expected for the $e^{\pm}$ hits. We define a shower width D as [11]

$$D = [\Sigma\, E_i(x_i - < x >)^2 / \Sigma\, E_i]^{1/2} \ , \qquad (3)$$

where x_i is a coordinate of the center of ith *SMD* row, and E_i is the energy deposited in this row; $< x >= (\Sigma x_i \cdot E_i)/\Sigma E_i$ is the energy weighted average of the position.

The estimates for the background from charged hadrons, obtained by Monte-Carlo simulations, are presented in Table 4 and in Figs. 8–10. With respect to hadrons, P_T^e in the figures and P_T^e*_cut* in the table represent their transverse momenta, as measured in the *EMC* which, as discussed above, are lower than actual P_T[4]. *CUT 1* includes only the "Energy-Momentum matching" and the "Isolation cut" criteria, but does not include "Shower width".

[4]Except of the original hadron spectra, generated by *PYTHIA/JETSET*, without any cuts, where P_T is a "true" hadron momentum provided by the event generator.

In *CUT 2*, the requirement of $D^2 < 10\,cm^2$ has been applied along with the two *CUT 1* criteria. *CUT 3* is the same as *CUT 2*, but with the requirement $D^2 < 4\,cm^2$. As in Tables 2 and 3, all event rates are normalized to W^+'s for $P_T^{e^+}\_cut = 10\,GeV/c$, without any other cuts applied.

Table 4. Background from high-P_T charged hadrons for $W^{\pm}$ production.

$P_T^{e^{\pm}}$ *cut*, GeV/c	CUT 1			CUT 2			CUT 3		
	W^+	W^-	Positive background	W^+	W^-	Positive background	W^+	W^-	Positive background
10	0.94	0.20	5.4	0.85	0.18	3.93	0.75	0.16	2.62
15	0.93	0.20	0.69	0.83	0.18	0.59	0.74	0.16	0.43
20	0.87	0.20	0.073	0.79	0.18	0.057	0.69	0.16	0.043
25	0.78	0.19	0.033	0.70	0.18	0.025	0.63	0.15	0.018
30	0.64	0.18	0.015	0.57	0.16	0.011	0.51	0.14	0.008
35	0.43	0.13	0.015	0.39	0.12	0.010	0.34	0.11	0.008

Preliminary[5] results for the background from high-P_T $\gamma-$quanta overlapping with charged hadrons in the *EMC/SMD* are also shown in Fig. 10. Such events were considered as a background to $W^{\pm}$ if the distance between the center of a shower from the γ and a charged hadron in the *EMC*, provided by tracking, was less than 1 cm. Otherwise an event was rejected. Two criteria from *CUT 1* were also applied.

5 Conclusion

The results presented here prove that a W^+ signal can be extracted in **STAR** at the acceptable background level of about 3–7%, while the detection efficiency due to applying cuts (CUT 2 & 3) drops by 15–25%. Background to W^- can be rejected to the level of 10–30% depending on the selection criteria.

More electron/hadron rejection may be achieved with the Silicon Vertex Tracker (*SVT*) due to the significant improvement of the momentum resolution in the tracking system for the high-P_T particles [1]. The capabilities of the dE/dx measurement in the *TPC* for $e^{\pm}$ selection [12] are also to be studied yet.

A number of other background sources, for example, open charm and beauty decays, are now under investigation, although they are expected to be at a significantly lower level than misidentified charged hadrons.

In spite of the lower production rate, we expect a Z^0 signal in **STAR** to be cleaner than $W^{\pm}$ due to one more constraint in the Z^0 signature: a reconstructed mass of the e^+e^- pair must be equal to the Z^0- boson mass.

[5]Low statistics.

Acknowledgments

We are pleased to express our appreciation to T. Hallman, J. Harris, M. LeVine and A. Yokosawa for the support of our visits to BNL. We are thankful to G. Bunce, A. Derevschikov, S. Nurushev, A. Pavlinov, J. Soffer, H. Spinka, M. Tannenbaum, A. Vasiliev, D. Underwood, and, in particular, to A. Yokosawa for the useful and encouraging discussions, to J. Murgatroyd for the help when preparing the paper, and to M. Rykov for the drawing.

References

[1] *The STAR collaboration*, Conceptual Design Report for the Solenoidal Tracker at RHIC (STAR), June 15, 1992.

[2] *The STAR EMC collaboration*, Conceptual Design Report for the Electromagnetic Calorimeter for the **STAR**, September 22, 1993.

[3] *M. J. Tannenbaum*, In the Proc. of the Polarized Collider Workshop, Penn State University, 1990, edited by J. Collins, S. Heppelmann and R. W. Robinett (AIP Conf. Proc. No 223, American Institute of Physics, NY, 1991), page. 201.

[4] *V. L. Rykov and A. A. Derevschikov*, Internal RSC Report RSC-BNL/IHEP-4, August 1992.

[5] *T. Sjostrand*, PYTHIA 5.6 and JETSET 7.3. Physics and Manual. CERN-TH.6488/92. W5035/W5044. May 1992.

[6] GEANT 3.15 User's Guide. CERN, 1992.

[7] *E. Eichten, I. Hinchliffe, K. Lane, C. Quigg*, Rev. Mod. Phys. **56** (1984) 579 and Erratum **58** (1986) 1065.

[8] *H. U. Bengtson and T. Sjostrand*, The LUND Monte Carlo Programs long writeup. Pool programs W5035/W5045/W5046/W5047/W5048. CERN, 1989.

[9] *RHIC Spin Collaboration*, Proposal on Spin Physics Using the RHIC Polarized Collider, August 14, 1992, corrected September 1992; Proposal Update dated September 2, 1993, corrected October 11, 1993, submitted to the BNL PAC October, 1993; and references therein.

[10] *B. V. Chuiko et al*, Preprint IHEP 92-104, Protvino, 1992 (To be published in NIM).

[11] *R. K. Bock et al.*, Data Analysis Techniques for High-Energy Physics Experiment. Cambridge University Press, 1990.

[12] *K. Keinknecht*, Phys. Rep. **84** (1982) 85; *D. Decamp et al, (ALEPH Collaboration)*, Nucl. Instr. & Meth., **A294** (1990) 121; *D. Decamp et al, (ALEPH Collaboration)*, Phys. Lett., **B244** (1990) 551.

Figure Captions

Fig. 1. A cross-sectional view of one-half of the **STAR** detector. Notations:

EMCB – Electromagnetic Barrel Calorimeter;
EMCEC – Electromagnetic Endcup Calorimeter (**STAR** upgrade);
TPC – Time Projection Chamber;
SVT – Silicon Vertex Tracker (**STAR** upgrade).

Fig. 2. Pseudorapidity distribution for $e^{\pm}$ from $W^{\pm}$ decay.

Fig. 3. P_T distribution for $e^{\pm}$ from $W^{\pm}$ decay for $|\eta| \leq 0.95$.

Fig. 4. P_T distribution for highest P_T $e^{\pm}$ from Z^0 decay for $|\eta| \leq 0.95$.

Fig. 5. P_T distribution for $e^{\pm}$ from $W^{\pm}$ decay and background from Z^0.

Fig. 6. Generated hadron spectrum (solid) for $P_T > 10\,Gev/c$, $|\,\eta\,| \leq 0.95$ and a corresponding spectrum measured with *EMC* (dashed).

Fig. 7. Rejection power for the "Energy-Momentum matching" criterion. The solid (dashed) histogram and line correspond to the rejection power without (with) "Energy-Momentum matching" criterion applied (lines are polynomial fits to histograms).

Fig. 8. Charged hadron background vs. P_T before and after applying *CUT 1* rejection criteria (see text) along with $e^{\pm}$ from $W^{\pm}$ decays.

Fig. 9. The same as Fig. 8, but for *CUT 2*.

Fig. 10. The same as Fig. 8 , but for *CUT 3*. Also shown the background from γ-quanta overlapping with positive hadrons.

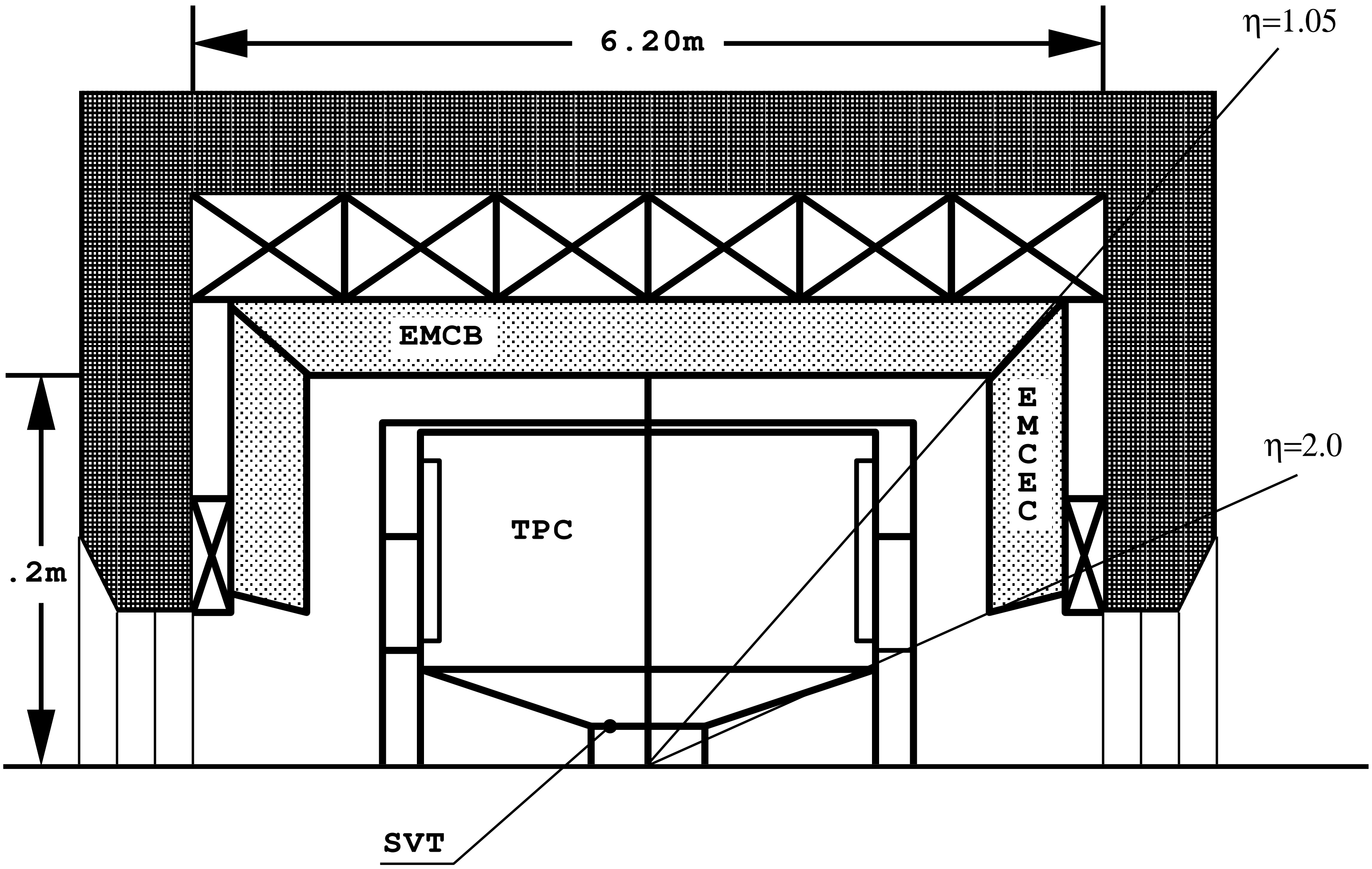

Fig.1

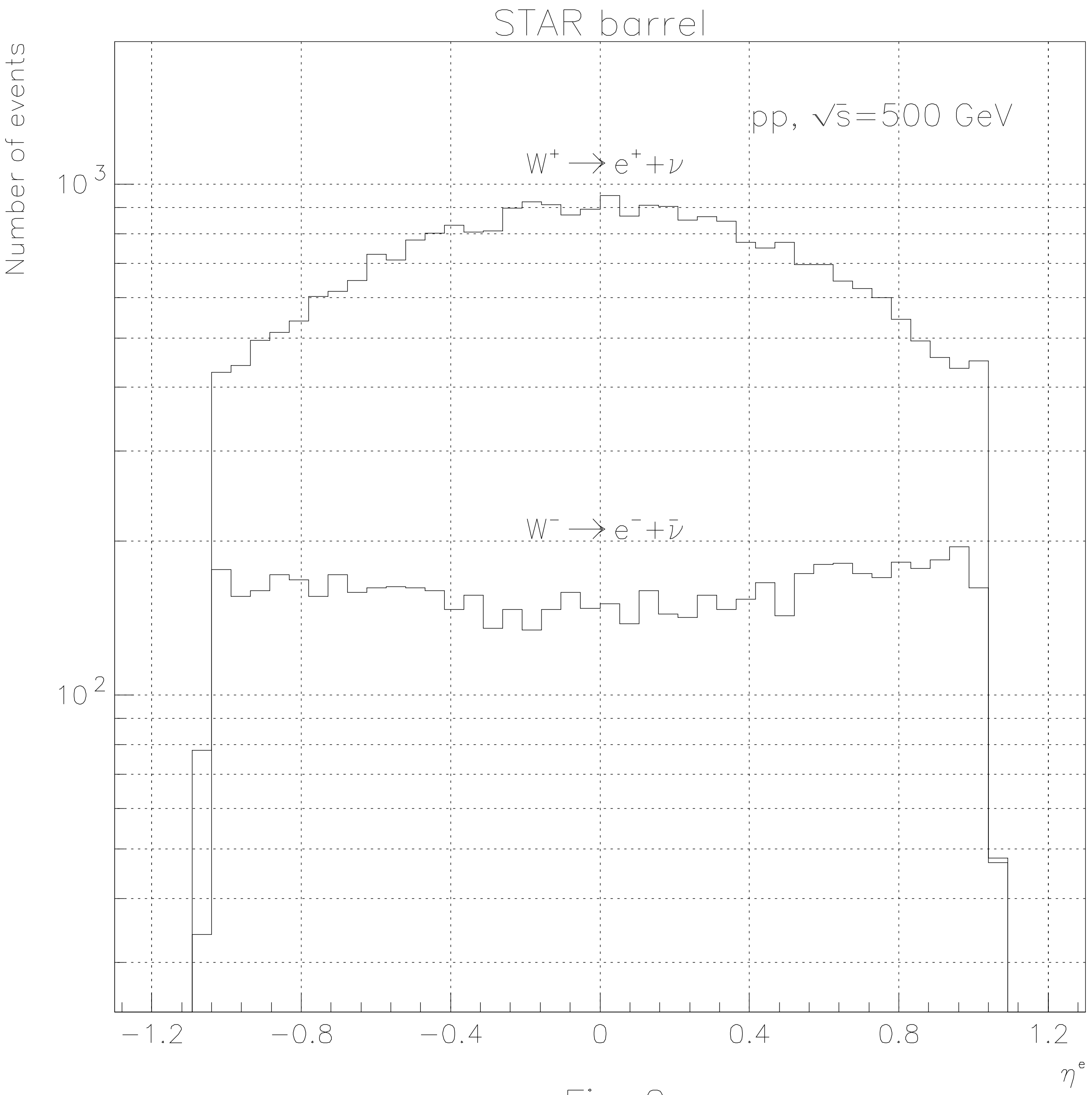
STAR barrel
Number of events
pp, √s=500 GeV
W⁺ → e⁺+ν
W⁻ → e⁻+ν̄
10³
10²
−1.2
−0.8
−0.4
0
0.4
0.8
1.2
η^e

Fig. 2

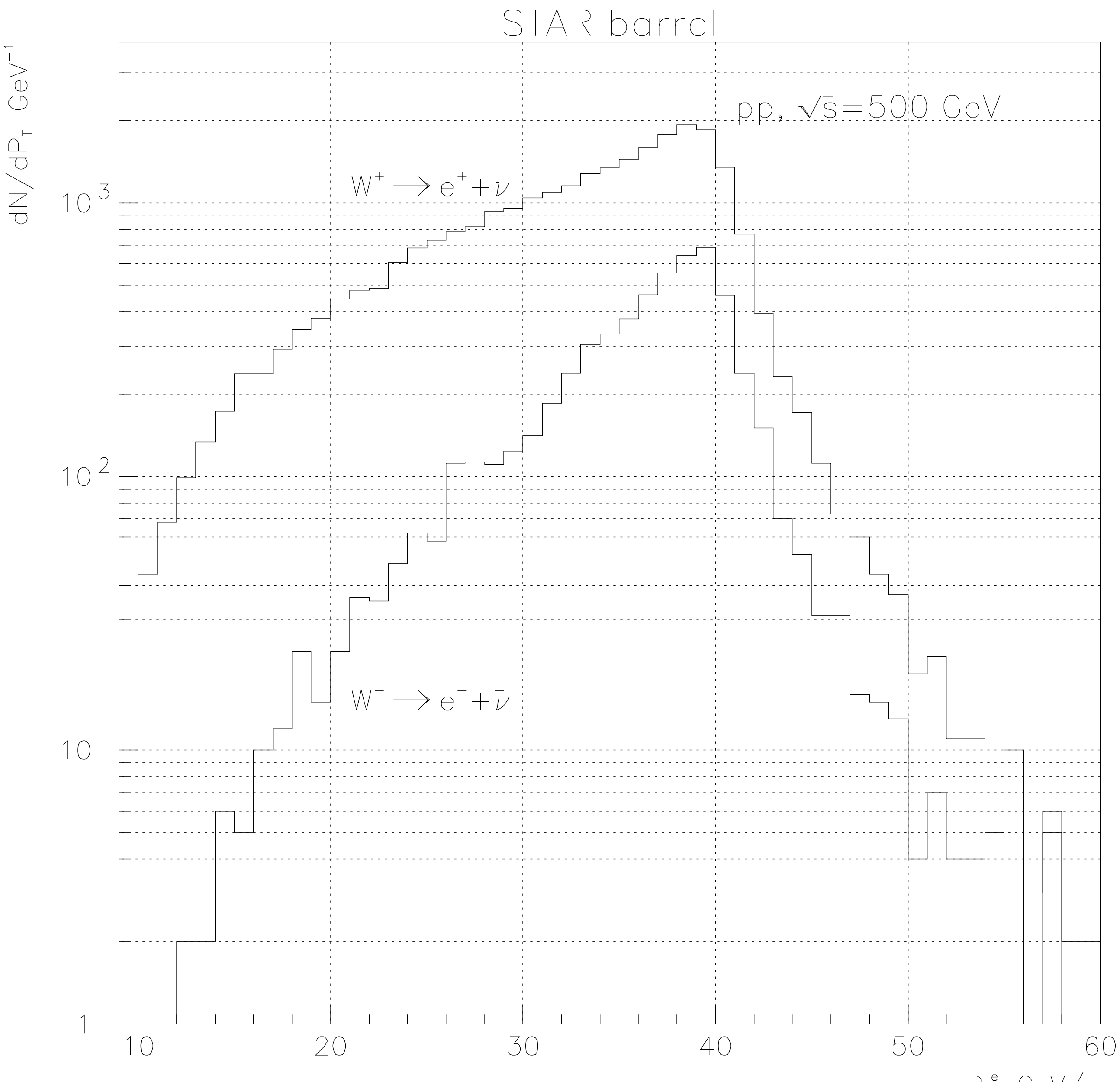
STAR barrel
pp, √s=500 GeV
$W^+ \longrightarrow e^+ + \nu$
$W^- \longrightarrow e^- + \bar{\nu}$
dN/dP_T GeV^-1
10^3
10^2
10
1
10
20
30
40
50
60
P_T^e GeV/c

Fig. 3

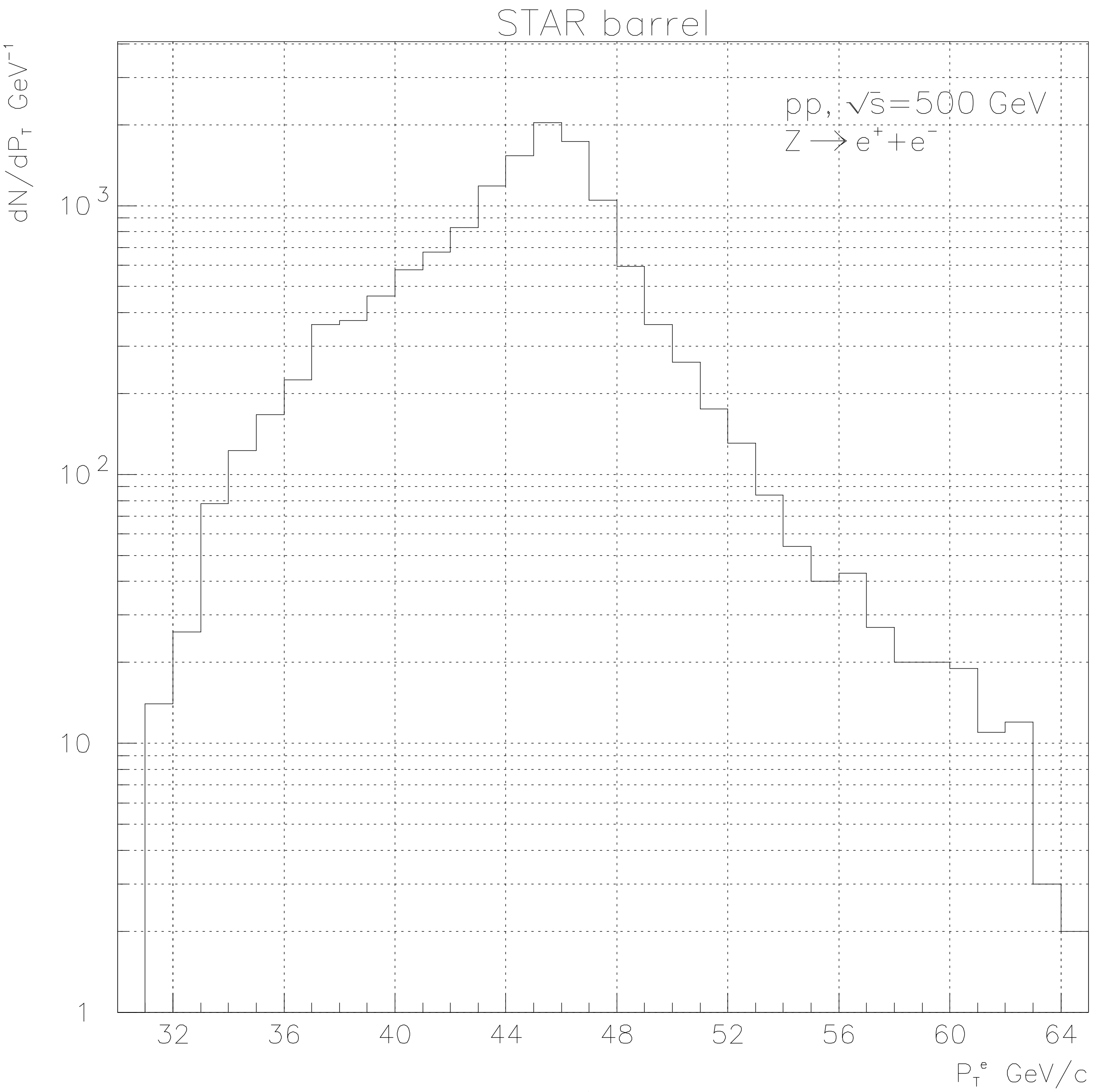
STAR barrel
pp, √s=500 GeV
Z → e⁺+e⁻
dN/dP_T GeV⁻¹
10³
10²
10
1
32
36
40
44
48
52
56
60
64
P_T^e GeV/c

Fig. 4

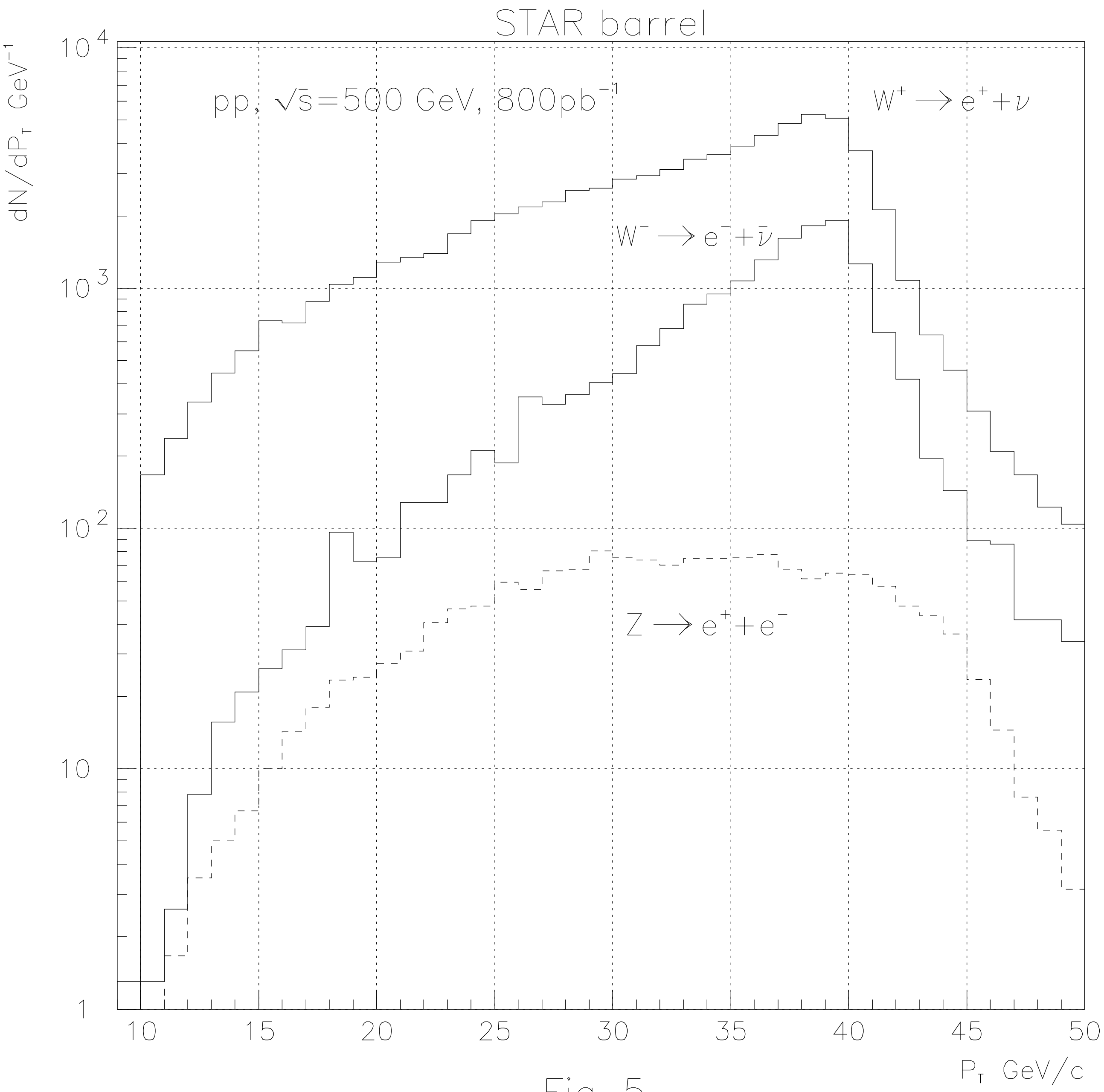
STAR barrel
pp, √s=500 GeV, 800pb⁻¹
W⁺ → e⁺+ν
W⁻ → e⁻+ν̄
Z → e⁺+e⁻
dN/dP_T GeV⁻¹
10⁴
10³
10²
10
1
10
15
20
25
30
35
40
45
50
P_T GeV/c

Fig. 5

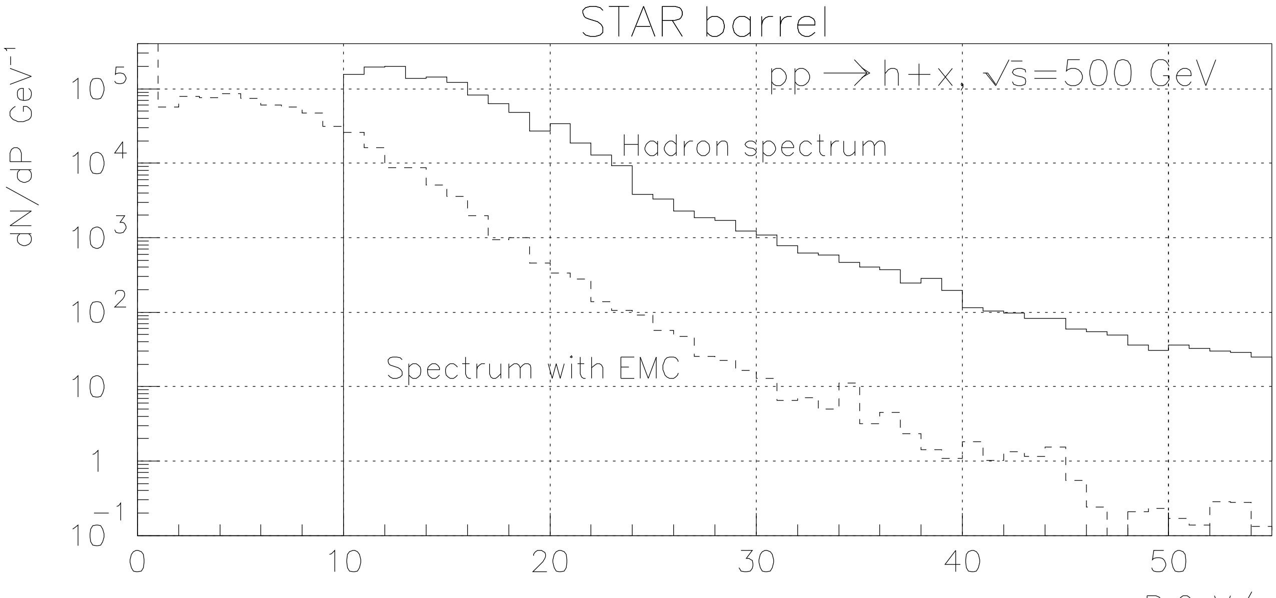
STAR barrel
pp → h+x, √s=500 GeV
Hadron spectrum
Spectrum with EMC
dN/dP GeV⁻¹
P GeV/c

Fig. 6

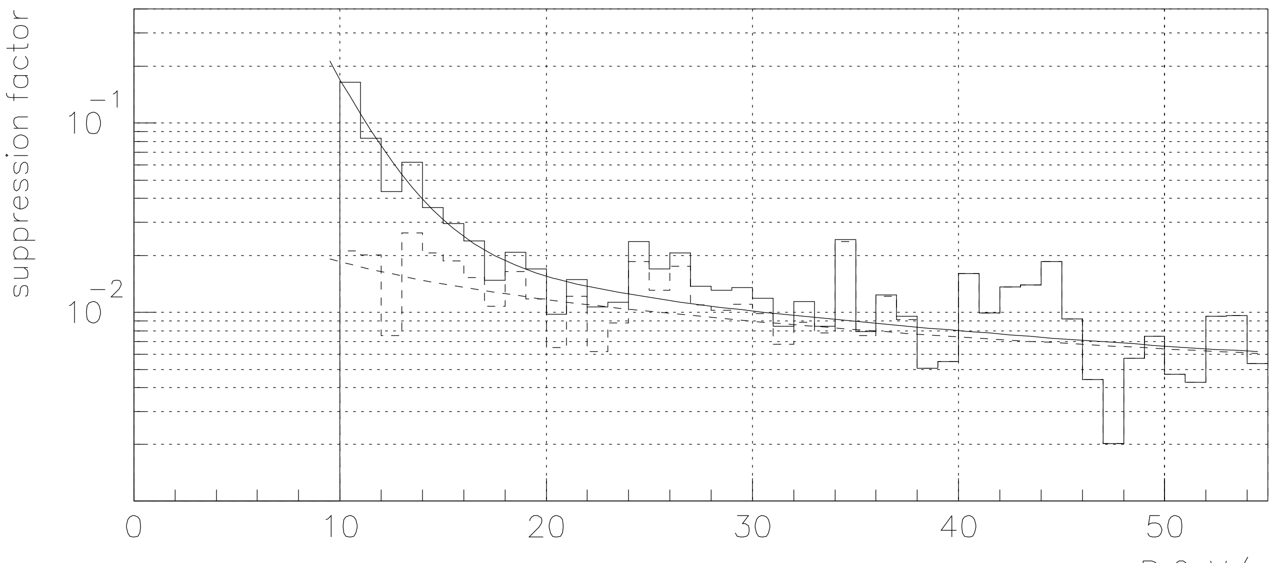
suppression factor
P GeV/c

Fig. 7

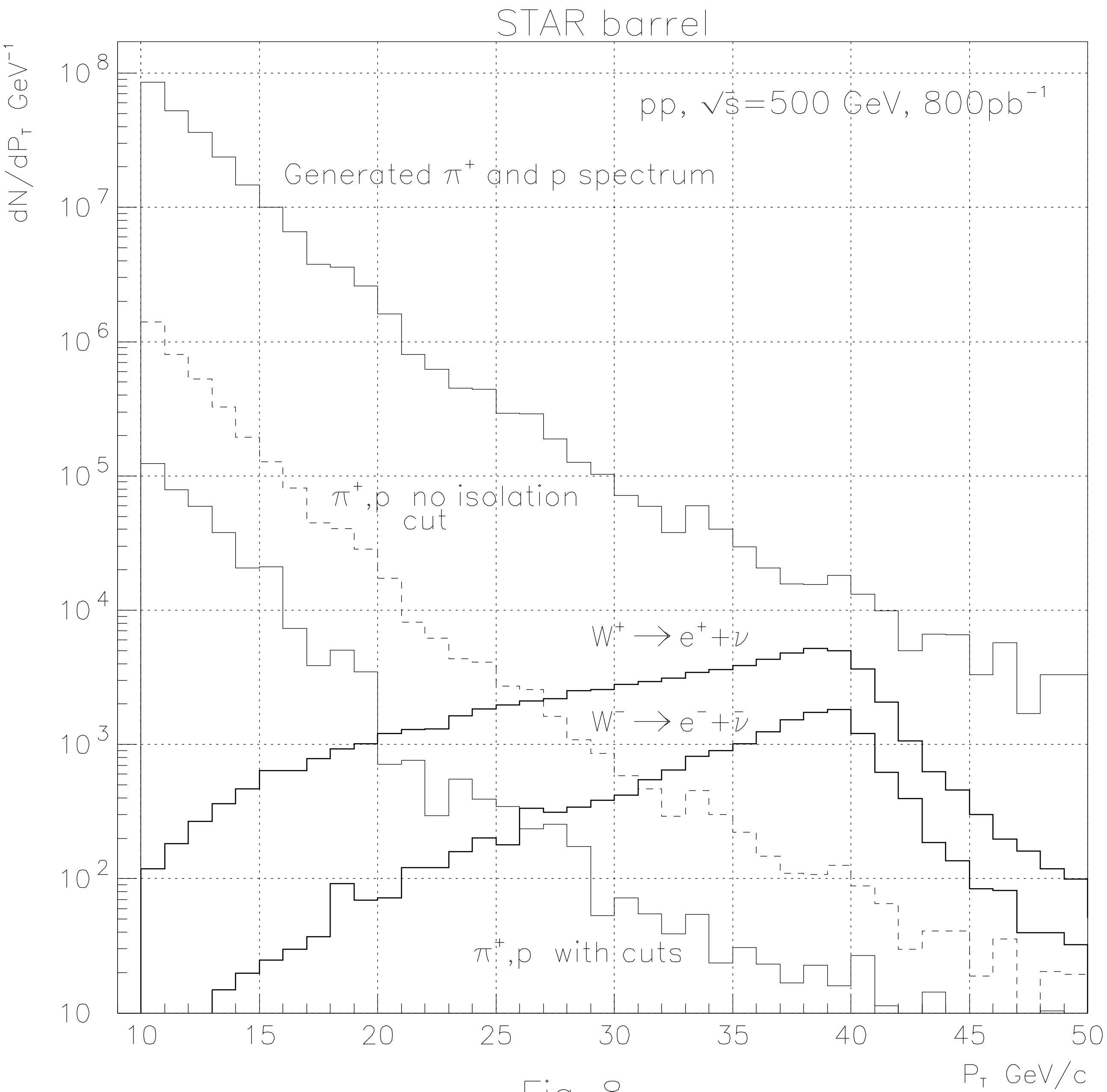

STAR barrel
dN/dP_T GeV^-1
pp, √s=500 GeV, 800pb^-1
Generated π+ and p spectrum
π+,p no isolation cut
W+ → e+ + ν
W- → e- + ν̄
π+,p with cuts
10^8
10^7
10^6
10^5
10^4
10^3
10^2
10
10
15
20
25
30
35
40
45
50
P_T GeV/c

Fig. 8

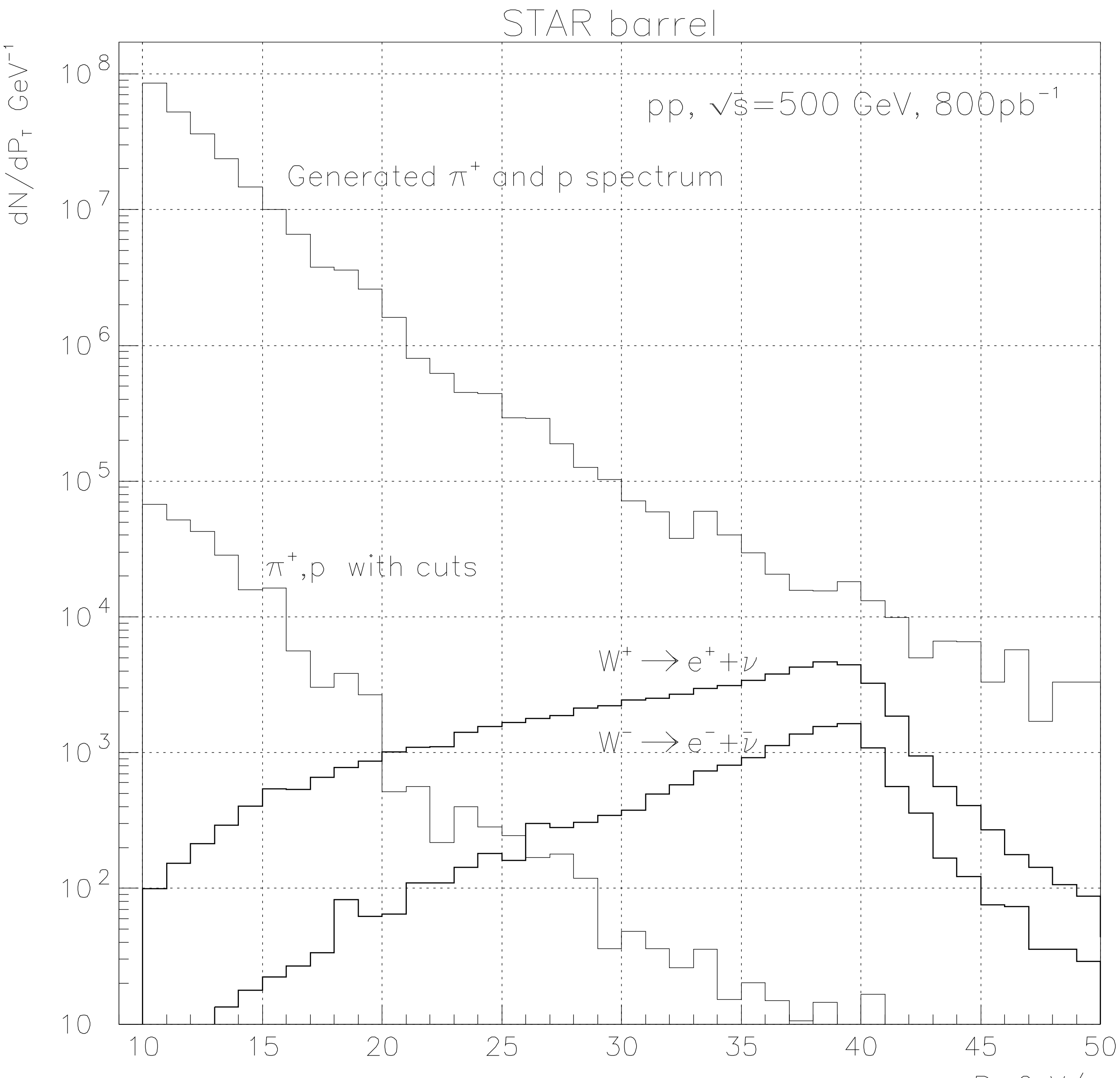
STAR barrel
dN/dP$_T$ GeV^{-1}
pp, $\sqrt{s}$=500 GeV, 800pb^{-1}
Generated π^+ and p spectrum
π^+,p with cuts
$W^+ \rightarrow e^+ + \nu$
$W^- \rightarrow e^- + \bar{\nu}$
10
15
20
25
30
35
40
45
50
P$_T$ GeV/c
10
10^2
10^3
10^4
10^5
10^6
10^7
10^8

Fig. 9

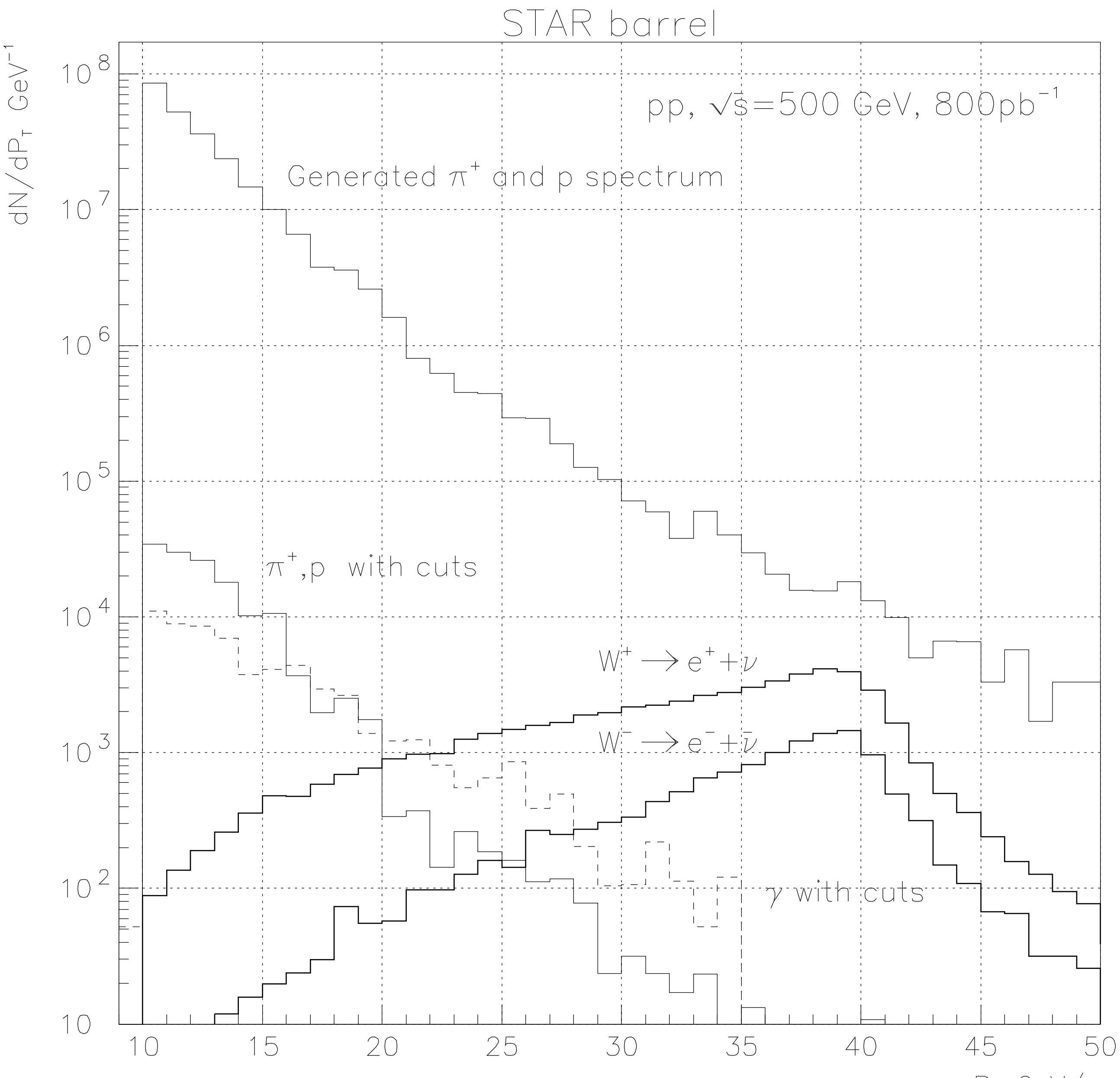
STAR barrel
pp, $\sqrt{s}$=500 GeV, 800pb^{-1}
Generated π^+ and p spectrum
π^+,p with cuts
$W^+ \rightarrow e^+ + \nu$
$W^- \rightarrow e^- + \bar{\nu}$
γ with cuts
dN/dP$_T$ GeV^{-1}
P$_T$ GeV/c
10
15
20
25
30
35
40
45
50
10^8
10^7
10^6
10^5
10^4
10^3
10^2
10

Fig. 10